Supplementary file of "Synergism of artificial intelligence and techno-economic for sustainable treatment of methylene blue dye-containing wastewater by photocatalysis"

Preliminary results on MB removal using dark and light conditions.

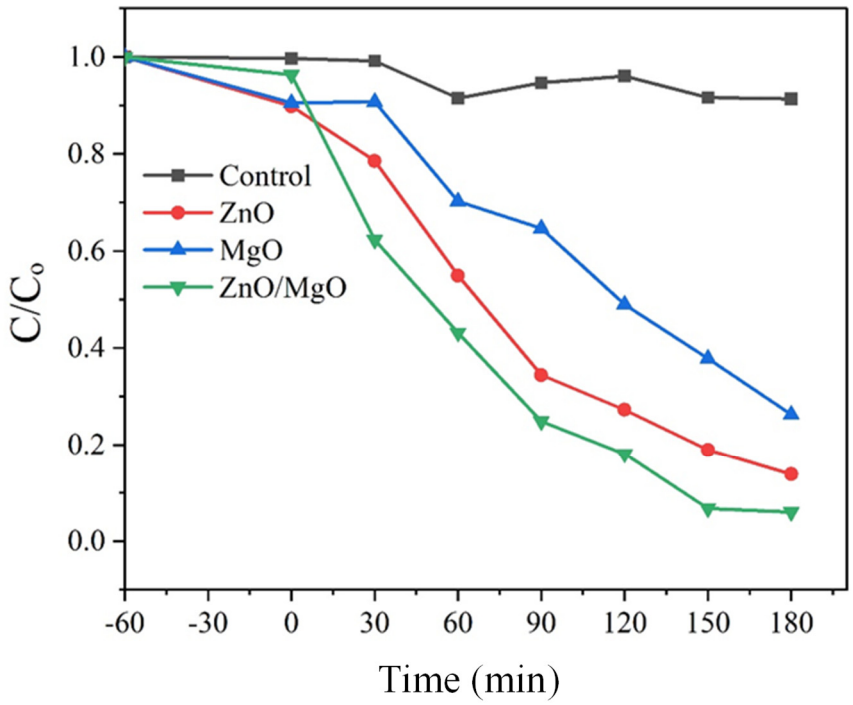

Figure S1. Initial photocatalysis experiments under light irradiation.

Fig. S1 shows the photocatalytic degradation curves generated for ZnO, MgO, and the ZnO/MgO nanocomposite. The results of the photocatalytic experiments showed that, with the addition of catalyst to the MB solution in the presence of solar-simulated UV light, the nanocomposite displayed the highest and fastest MB removal efficiency in 180 min at 94.01%. The performance of this catalyst was followed by that of pure ZnO with an MB removal efficiency of 88.34% in 180 min. The pure MgO displayed the lowest MB removal efficiency of 86.20% within 180 min. The superior performance of the composite material was indicative of good synergistic performance resulting from the combination of ZnO and

MgO. The mechanism followed by the composite material for MB removal was governed by Equations S1, S2, and S3 [1]:

$$ZnO@MgO \xrightarrow{h\nu} e_{CB} + h_{VB} \quad \text{(Eq. S1)}$$

$$h_{VB} + H_2O \longrightarrow \bullet OH + H^+ \quad \text{(Eq. S2)}$$

$$(h_{VB}, \bullet OH, e_{CB}, O_2^{\bullet -}) + MB \longrightarrow Degradation\ intermediates + CO_2 + H_2O \quad \text{(Eq. S3)}$$

The enhanced performance of the nanocomposite could be a result of factors such as reduced electron–hole recombination, successful reduction in the band gap energy of the nanocomposite material, and an increased number of active sites on the photocatalyst surface.

A photolysis experiment control in Fig. S1 was also conducted. The results showed that the contribution of photolysis towards MB removal after 180 min was only ≈8.5%.

BET Characterization

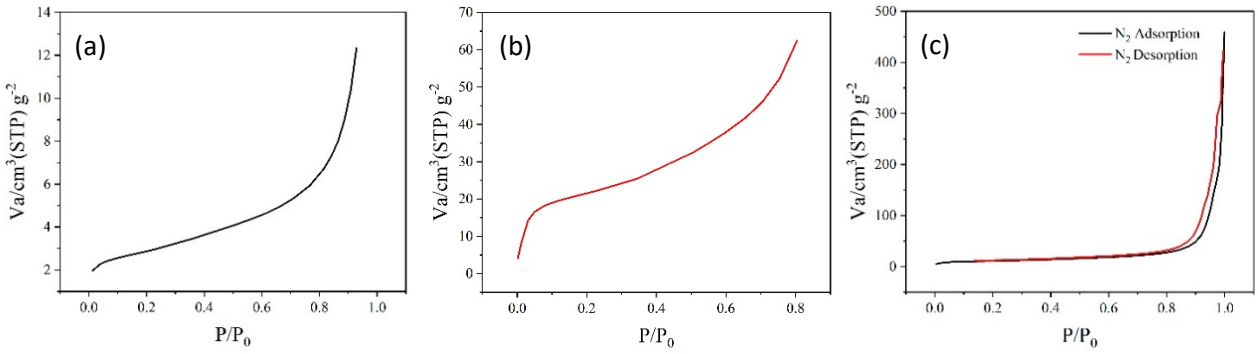

Figure S2. N_2 adsorption–desorption isotherms of (a) ZnO, (b) MgO, and (c) ZnO/MgO.

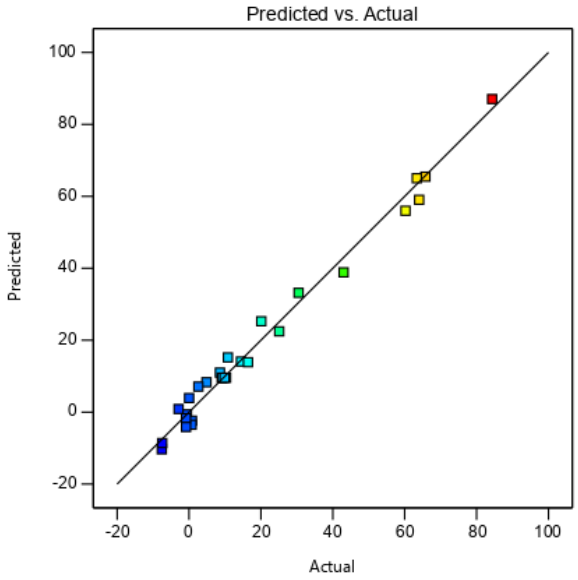

Figure S3. Plot of actual versus predicted MB removal efficiencies.

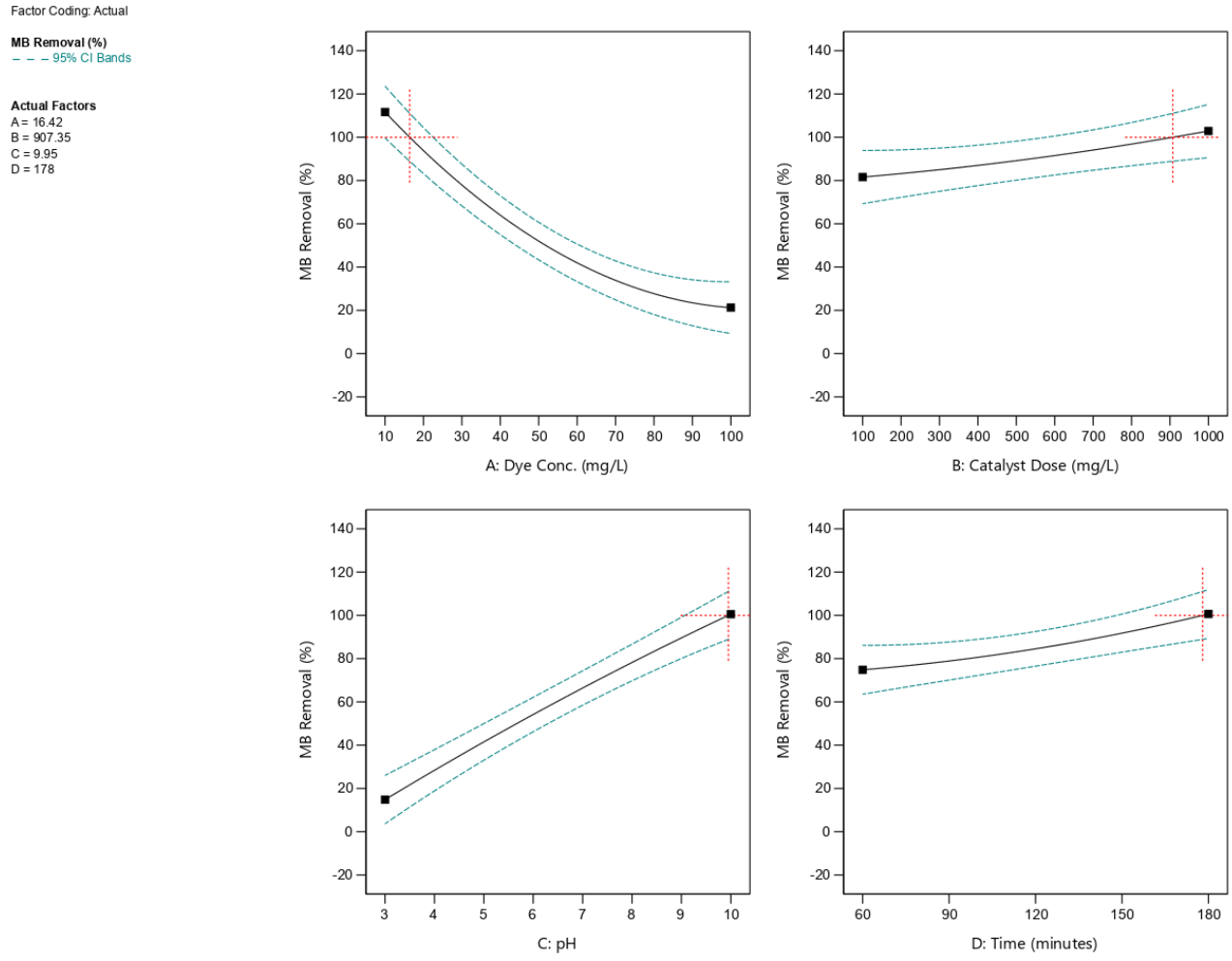

Figure S4. Optimization of photocatalysis independent variables using the response surface methodology (RSM) based on the quadratic regression model.

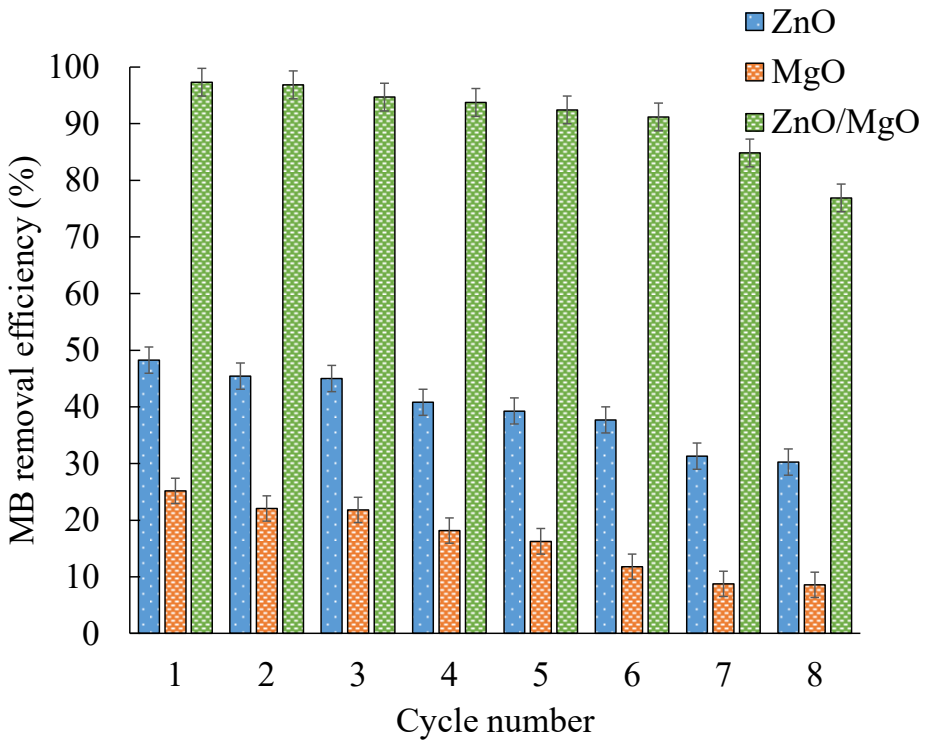

Figure S5. Recyclability of the photocatalyst material.

Sensitivity analysis on cost estimation calculations.

In order to determine the effect on the treatment cost of variations to various costs estimated in the economic analysis, a sensitivity analysis based on what-if scenarios was carried out. The analysis varied the cost of photocatalytic reactor, chemical costs, electrical consumption costs, and water consumption costs from -30% to 30%, as shown in Fig. S6.

The results of the analysis showed that varying the cost of installation had the most significant impact on the total cost of treatment. Increasing the installation costs by 30% resulted in a 12.47% increase in the treatment cost to USD 9.72/m^3. Moreover, a 30% reduction in the installation cost had a significant impact on the treatment cost. This led to a 10.62% reduction in the treatment cost to USD 7.29/m^3. Variations in the cost of electricity consumption also revealed a significant impact on the total treatment cost, where a 30%

increase in the cost of chemicals resulted in an 11.5% treatment cost rise to USD 9.61/m^3. Similarly, a 30% electrical cost reduction revealed a 14.93% reduction in the treatment cost to USD 7.40/m^3. In the case of the cost of chemicals and water consumption costs, variations in cost revealed insignificant changes in the overall cost of treatment compared with the base case scenario.

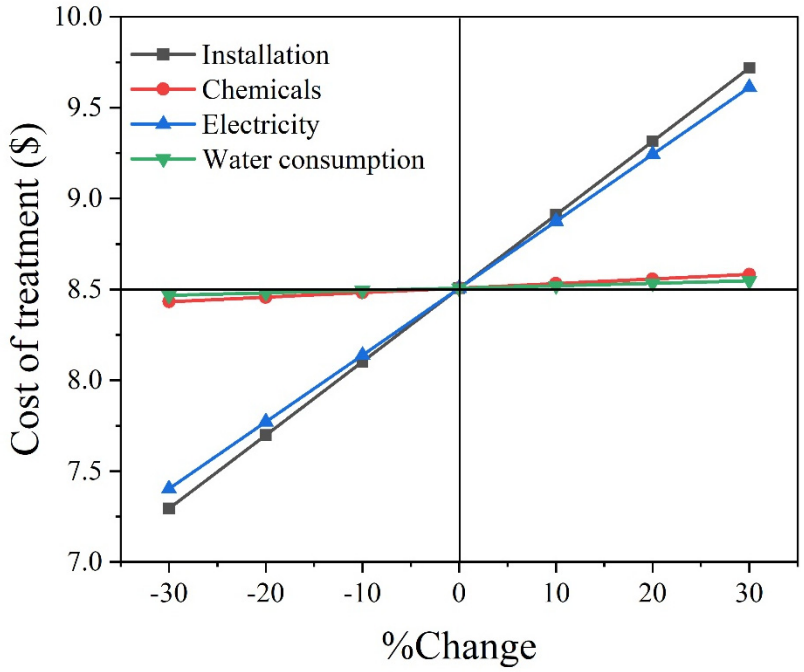

Figure S6. Effect of variation from -30% to 30% on the total treatment cost.

Table S1. Chemicals and reagents used for experimental procedures. All chemicals were utilized in the experiments without further purification.

Chemical/reagent	Specification	Source

Magnesium Chloride Hexahydrate	$MgCl_2 \cdot 6H_2O$; ≥ 99% purity	Tekkim Kimya Labs, Turkey
Zinc sulfate heptahydrate	$ZnSO_4 \cdot 7H_2O$	El Nasr pharmaceutical chemicals company in Egypt
Purified sodium hydroxide pellets	NaOH; ≥ 97% purity	SD Fine Chemicals, India
Sulfuric acid	H_2SO_4; 97% purity	PioChem Company in Egypt
Methylene blue powder	$C_{16}H_{18}ClN_3S$; 99% purity	El Nasr Pharmaceutical Chemicals, Egypt
Nylon syringe filters	0.22 μm	ChromTech Ltd., United Kingdom

30

31

Table S2. Selection of best number of neurons in the hidden layer (N) and transfer function based on the smallest MSE of different ANN models for predicting MB removal efficiencies. Here, *trainoss*: one step secant; *traincgb*: conjugate gradient with Powell–Beale restart; *trainbfg*: Broyden–Fletcher– Goldfarb–Shanno (BFGS) quasi-Newton; *trainlm*: Levenberg–Marquardt; *trainscg*: scaled conjugate gradient; *traincgf*: Fletcher–Powell conjugate gradient; *traingd*: gradient descent back-propagation.

Hidden neurons	Training function	Iteration	MSE	Coefficient of determination (R^2)			
				Training	Validation	Test	Overall
4	*trainlm*	11	28.32	0.9227	0.8747	0.4185	0.8173
6	*trainlm*	7	13.77	0.7347	1.0247	0.8363	0.7746
8	*trainlm*	5	11.20	0.9431	0.9925	0.9959	0.9464
10	*trainlm*	5	12.36	0.8664	1.0179	0.9029	0.8932
12	*trainlm*	5	17.64	0.9380	0.9472	0.9077	0.8193
8	*trainbfg*	7	154.10	0.2438	0.7830	0.1382	0.2685
8	*traincgb*	103	112.51	0.5134	0.0557	0.1413	0.3151
8	*traincgf*	118	122.56	0.8448	0.0231	0.8248	0.6158
8	*trainoss*	40	49.82	0.8899	1.0104	0.5475	0.5096
8	*trainscg*	28	25.88	0.8759	1.1052	0.5716	0.7575
8	*traingd*	10	36.30	0.4218	0.7362	0.2365	0.3748

Table S3. Optimum weights and biases of the feed-forward back-propagation ANN (4–8–1) with *trainlm* training function used to predict the MB R(%).

Hidden layer node	Weight matrix between the input and the hidden layer ($W_{8\times4}$)				Hidden layer threshold ($B_{8\times1}$)
	$k = 1$	$k = 2$	$k = 3$	$k = 4$	
m= 5	-0.1249	-1.6200	-1.2346	-0.1047	2.5905
m= 6	1.7641	0.9902	0.7087	0.1158	-2.1585
m= 7	1.2449	0.8098	1.4198	-1.6486	-1.1836
m= 8	0.5427	-1.0484	-1.9836	1.1122	0.8453
m= 9	2.0849	-1.6122	-0.4756	-1.4836	-0.3590
m= 10	2.3620	-0.1016	-1.1756	-0.9851	1.5899
m= 11	-0.2738	0.7934	2.9975	-1.0515	-1.4511
m= 12	1.4727	1.1232	-0.6377	-1.8715	1.9483

Output layer node	Weight matrix between the hidden and the output layer ($W_{1\times8}$)								Output layer threshold ($B_{1\times1}$)
	m= 5	m= 6	m= 7	m= 8	m= 9	m= 10	m= 11	m= 12	
n = 13	0.0958	0.1502	-0.2655	-0.8599	0.0138	-0.7569	-0.5345	0.0231	-0.1513

References

[1] A. Ajmal, I. Majeed, R. N. Malik, H. Idriss en M. A. Nadeem, „Principles and mechanisms of photocatalytic dye degradation on TiO 2 based photocatalysts: A comparative overview,” *RSC Advances,* vol. 4, nr. 70, pp. 37003-37026, 2014.